RELATIVE RESPONSE TO LOW-ENERGY PHOTONS AND DETERMINATION OF INSTRUMENT CORRECTION FACTORS FOR PORTABLE RADIATION INSTRUMENTATION

A Thesis

by

DAVID ANDREW WAGONER

Submitted to the Office of Graduate Studies of
Texas A&M University
in partial fulfillment of the requirements for the degree of

MASTER OF SCIENCE

August 2010

Major Subject: Health Physics

RELATIVE RESPONSE TO LOW-ENERGY PHOTONS AND DETERMINATION OF INSTRUMENT CORRECTION FACTORS FOR PORTABLE RADIATION INSTRUMENTATION

A Thesis

by

DAVID ANDREW WAGONER

Submitted to the Office of Graduate Studies of
Texas A&M University
in partial fulfillment of the requirements for the degree of

MASTER OF SCIENCE

Approved by:

Co-Chairs of Committee,	Leslie A. Braby
	John W. Poston, Sr.
Committee Members,	James T. White
Head of Department,	Raymond J. Juzaitis

August 2010

Major Subject: Health Physics

ABSTRACT

Relative Response to Low-Energy Photons and Determination of Instrument Correction Factors for Portable Radiation Instrumentation. (August 2010)

David Andrew Wagoner, B.S., Francis Marion University

Co-Chairs of Advisory Committee: Dr. Leslie A. Braby
Dr. John W. Poston, Sr.

Practically all portable radiation instruments come from the manufacturer with a graph of photon energy response. However, many of these graphs are in log-log format which can disguise relatively large variations in response, particularly for low-energy photons. Additionally, many only include one specific orientation. Thus, in many cases, it is left up to the user to determine for which orientation and photon energies the instrument will be calibrated and ultimately used in the field. It is known that many instruments can have inconsistent responses below ~300 keV, which may lead to under or over-estimation of exposure rate. However, based on relative response plots, one can derive an instrument correction factor that can be applied to the measured exposure rate to yield a constant response curve and more accurately estimate the exposure rate.

Using a combination of irradiator systems, six different types of radiation instrumentation were irradiated with photons with energies from 38 to 1253 keV in various orientations. A calibrated ion chamber, in conjunction with an electrometer, was used to determine the conventionally true exposure rates for various x-ray beam codes and radionuclides contained in the irradiator systems. The conventionally true exposure

rates were compared to the measured values for each instrument type and relative response plots were constructed. These plots were used to determine an ideal orientation and correction factors were chosen for responses > $\pm$20%.

From the relative response plots, instrument correction factors are not necessary for the following; Eberline RO-20, Thermo RadEye B20, and Bicron Micro Rem LE. Correction factors of 0.7 and 1.5 should be applied for photons between 80 – 120 keV for the Eberline Teletector 6112B low and high-range detectors, respectively. A correction factor of 0.8 should be applied for photons below 120 keV for the Eberline RO-7-BM. For the Thermo Mk2 EPD, a correction factor of 1.25 should be applied for photons below 40 keV. The primary causes of under and/or over-responses were found to be window attenuation, varying interaction cross-sections, and the range of secondary electrons. Angular dependence and calibrations for specific applications are also discussed.

ACKNOWLEDGEMENTS

I would like to extend immense gratitude to Dennis Hadlock for being my mentor and sharing his wealth of knowledge throughout the course of this research. I would also like to thank Dante' Wells, Amber Dailey, and the technical staff at the Health Physics Instrument Calibration Facility at the Savannah River Site for their help and cooperation throughout this work.

I would like to thank my committee chair, Dr. Leslie Braby, and my committee members, Dr. John Poston Sr. and Dr. James White for their guidance and support during the writing and submission of this work.

Finally, thanks to my parents, Lee and Lori Locklair for their continuous support and encouragement throughout the duration of my undergraduate and graduate career.

TABLE OF CONTENTS

Page

LIST OF FIGURES

FIGURE Page

LIST OF TABLES

CHAPTER I

INTRODUCTION

Soon after the discovery of radiation and radioactivity many different detection methods were developed to accurately quantify the energy deposited by ionizing radiation. Many of these detection methods are still used today with little modification to their original design. The most common are the ion chamber, Geiger-Mueller tube, and scintillation detectors. A more modern detector that has recently become commercially available incorporates the use of rugged silicon diode detectors. Through the years it has become necessary to develop compact and portable instruments based on these detectors.

With the onset of nuclear power and the increasing use of radioactive materials, portable radiation instrumentation has become a crucial component of radiation protection programs when work is being performed with or around radioactive material. Perhaps of greater importance is the ability for these instruments to accurately measure exposure or dose equivalent rate. In most situations this is easily achieved, but when there are many different source terms positioned throughout an area emitting a wide range of energies, the accuracy of these instruments can quickly degrade.

Practically all portable radiation instruments come from the manufacturer with a

---

This thesis follows the style of *Health Physics*.

technical reference data sheet including a graph of photon energy response. However, many of these graphs are in log-log format, which can disguise relatively large variations, particularly in the low-energy portion of the graph. Additionally, many only include one specific orientation. Some instruments can have up to four orientations in which they can be calibrated and applied in different radiation fields. Thus, in many cases, it is left up to the user to determine for which orientation and range of photon energies the instrument will be calibrated and ultimately used in the field.

In this study, the relative response of six different instrument types to photons from 38 keV to 1253 keV in various orientations was measured and plotted. Based on these results an ideal orientation was chosen and instrument correction factors were determined where necessary. The origin of under and/or over-responses is analyzed and discussed.

CHAPTER II

BACKGROUND

Irradiator Systems

Irradiators can be fairly complex systems usually containing a high radiation source, whether it is a radionuclide or an x-ray machine, and a remotely controlled linear positioning system capable of moving on a variety of axes relative to the source. These systems are very useful in that they can be used to carry out experiments and calibrations using high-intensity radiation sources while the worker using them receives zero radiation dose.

There are three different irradiators used in this study; a Low-Scatter, Americium-241, and an x-ray irradiator. The Low-Scatter irradiator contains assorted strength Cesium-137 and Cobalt-60 sources, which are traditionally used for instrument calibrations. The effective energies of the photons emitted from this irradiator are 662 keV and 1253 keV, respectively. The Americium-241 irradiator contains a circular array of seven, one curie Americium-241 sources emitting a 59.5 keV photon. The x-ray irradiator is composed of an industrial tungsten anode tube head connected to a 320 kV high voltage power supply. By adjusting the added filtration and the voltage applied to the tube head, this system is capable of producing many different radiation fields.

The National Institute of Standards and Technology has specified several combinations of additional filtration and applied tube head voltage known as 'beam codes' to create particular radiation fields. For this study, a wide range of mono-

energetic photon energies is desired. Thus, beam codes were chosen based on the homogeneity coefficient and effective energy. The homogeneity coefficient is a measure of how monoenergetic a beam is. Beam codes begin with one of the following letters L, M, or H, corresponding to low, medium or heavy filtration. Heavily-filtered beams have the highest homogeneity coefficients, therefore a range of H series beam codes was appropriately chosen. The radionuclides, x-ray beam codes, and their respective effective energies chosen and used in this study are listed in Table 1.

Table 1. Radiation sources and their respective effective energies.

Source	Effective Energy (keV)
H50	38
Am-241	59.5
H100	80
H150	120
H200	166
H250	211
H300	252
Cs-137	662
Co-60	1253

Measurement Equipment

Air equivalent ion chambers are very reliable and can accurately measure the exposure rate from a radiation source. Many laboratories have ion chambers calibrated by the National Institute of Standards and Technology and utilize them as transfer

standards for determining conventionally true exposure rates. This section describes the essential measurement equipment used to determine the conventionally true values for the radiation sources listed in Table 1.

An Exradin A4 air equivalent ion chamber with a collecting volume of 30 cm^3 vented to the atmosphere was used to determine the conventionally true exposure rates. This particular ion chamber is a spherical detector with a wall thickness of 0.25 cm composed of C552 air-equivalent plastic. The ion chamber was calibrated by the National Institute of Standards and Technology. The x-ray beam codes and the corresponding calibration coefficients are listed in Table 2. A Keithley Model 6517 electrometer, connected via triaxial cable with BNC connectors, supplied -500 V to the ion chamber and was used to measure the charge collected per unit time on the anode due to exposure to ionizing radiation.

Table 2. Exradin A4 ion chamber calibration coefficients determined by the National Institute of Standards and Technology (NIST 2008).

Beam Code	Calibration Coefficient (Gy/C) at Standard Temperature and Pressure	Calibration Distance (cm)
H50	1.051E+06	100
H100	1.059E+06	100
H150	1.061E+06	100
H200	1.064E+06	100
H250	1.069E+06	100
H300	1.072E+06	100

Equation 1 can be used to calculate the electrical current based on the electric charge collected in the ion chamber and measured by the electrometer:

$$I = \frac{Q}{t} \tag{1}$$

where: I = electrical current;
Q = electrical charge (nC); and
t = time (s).

Since the ion chamber is vented to the atmosphere and the calibration coefficients are intended for measurements at standard temperature and pressure, a temperature and pressure correction factor must be applied to the exposure rate calculations. The equation used in this work is:

$$TP_{corr.factor} = \left(\frac{T_{measured} + 273.15}{295.15} \right) \left(\frac{760 mm\ Hg}{P_{measured}} \right) \tag{2}$$

where: $TP_{corr.factor}$ = standard temperature and pressure correction factor;
$T_{measured}$ = measured temperature (˚C); and
$P_{measured}$ = measured pressure (mm Hg).

Substituting the values calculated with Equations 1-2 into Equation 3, one can calculate the conventionally true exposure rate:

$$\dot{X} = \left(\left| I - I_{leakage} \right|\right)\left(TP_{corr.factor}\right)\left(CF\right) \quad (3)$$

where: $\dot{X}$ = exposure rate (mR/hr); and

CF = ion chamber energy calibration factor.

Americium-241 Calibration Factor

The National Institute of Standards and Technology does not provide a calibration coefficient for the low-energy photon (59.5 keV) emitted from Americium-241. Thus, to use this radionuclide as a practical source, a calibration coefficient for 59.5 keV must be accurately determined. Since this energy lies between the effective energies of the x-ray beam codes for which the ion chamber is already calibrated, a calibration coefficient can be interpolated from a plot of calibration coefficient vs. effective energy. Once this is determined, the same equations can be applied to calculate the conventionally true exposure rates.

Basic Radiation Detector Theory

There is a variety of different types of detectors in use today. However, in the end, they all achieve the same goal, to generate an electrical signal as a result of photon interactions with a medium. This section explains the basic mechanisms by which common radiation detectors ultimately achieve the goal of converting photon energy into an electrical signal.

One of the most widely employed instruments used to detect ionizing radiation is a Geiger-Mueller detector. A Geiger-Mueller detector is a sealed chamber filled with a

low-pressure gas. An electric field is created within the gas by applying a high voltage between two electrodes. When radiation interacts with the chamber, the gas becomes ionized and the subsequent electrons collide with other gas molecules creating a Townsend avalanche of electrons. The potential difference is set to a value high enough to cause the avalanche to expand over the entire detector anode. The resulting electrical pulses can be used to measure the fluence rate of the radiation. The major drawback with this type of detector is that every Townsend avalanche, or interaction, produces the same pulse height. Because of this, Geiger-Mueller detectors cannot discriminate between photon energies (Knoll 2000). When used as dosimeters, most Geiger-Mueller detectors are encased in an energy compensating case to combat the over responses observed at low energies.

Another common and more accurate type of detector used to measure photon exposure rates is the ionization chamber. Since the definition of exposure rate is the amount of charge created by ionizing radiation in air, it is essential to collect the ionizations created in a finite volume of air as accurately as possible. Ion chambers used for this type of measurement have 'air equivalent' walls constructed of conductive plastic with an effective atomic number close to that of air. The walls must be thick enough to establish electronic equilibrium, in which the number of secondary electrons reaching the active volume is independent of the wall thickness (Knoll 2000). To automatically compensate for changes in air density, the chamber is vented to the atmosphere with air as the fill gas. A high voltage is applied between the cathode and anode to create a uniform electric field within the chamber. Photons interact with the

chamber wall or with the air in the chamber, ejecting energetic electrons into the active volume. These electrons interact with air molecules producing ion pairs. The negative ions are collected by the anode and an electrometer circuit measures the change in voltage across a resistor in series with the anode, effectively measuring the rate of charge collection. The voltage change can be correlated with the incident photon exposure rate.

Because the atomic composition of most organic scintillation materials is close to that of tissue, they are frequently used to measure dose equivalent rate. When photons interact with scintillation materials, the secondary electrons ionize or excite the molecules within the material. The molecules quickly de-excite back to the ground state resulting in the emission of visible light. The visible light interacts with the photocathode of a photomultiplier tube at one end of the scintillator, where its absorption results in emission of low-energy photoelectrons. The photoelectrons are accelerated and multiplied through secondary electron emission at a series of equally spaced dynodes, creating an electrical signal.

Silicon diode detectors are becoming a popular choice for measuring dose equivalent rate. A PiN diode detector consists of a lightly-doped, intrinsic region in between heavily-doped p-type and n-type semiconductors. When an electric potential is placed across the contacts of the diode (p-type and n-type regions) the electron-hole pairs in the intrinsic region move to the respective p-type and n-type regions, resulting in a depleted intrinsic region (Knoll 2000). When radiation interacts with the depleted intrinsic region, ion pairs are created and promptly swept out of the intrinsic region by the electric field to the respective p-type or n-type regions of the diode. The movement

of the electrons out of the intrinsic region generates the electrical signal. As with the Geiger-Mueller detector, energy compensating cases are also commonplace.

Portable Radiation Instrumentation Tested

Six different types of portable radiation instrumentation were tested in this study. Their calibration orientations and available technical specifications are discussed in the following section. The table on page 17 provides a summary of basic characteristics and the number tested for each instrument type.

The Eberline RO-20, pictured in Figure 1, is a portable ion chamber intended to measure exposure rate due to photons and beta radiation. The detector has an active volume of 220 cm^3 vented to the atmosphere with 0.510 cm thick phenolic walls. The detector is housed in a 0.160 cm thick aluminum case. The total density thickness in the side and front orientations is 1000 mg/cm^2. In the bottom orientation, there is a movable 0.790 cm thick phenolic beta slide in front of two very thin Mylar windows providing a total density thickness of 1000 mg/cm^2 with the beta slide closed. With the beta slide in the open position, the Mylar windows provide a density thickness of 7 mg/cm^2. This instrument is calibrated to Cesium-137 in the bottom, slide-closed configuration.

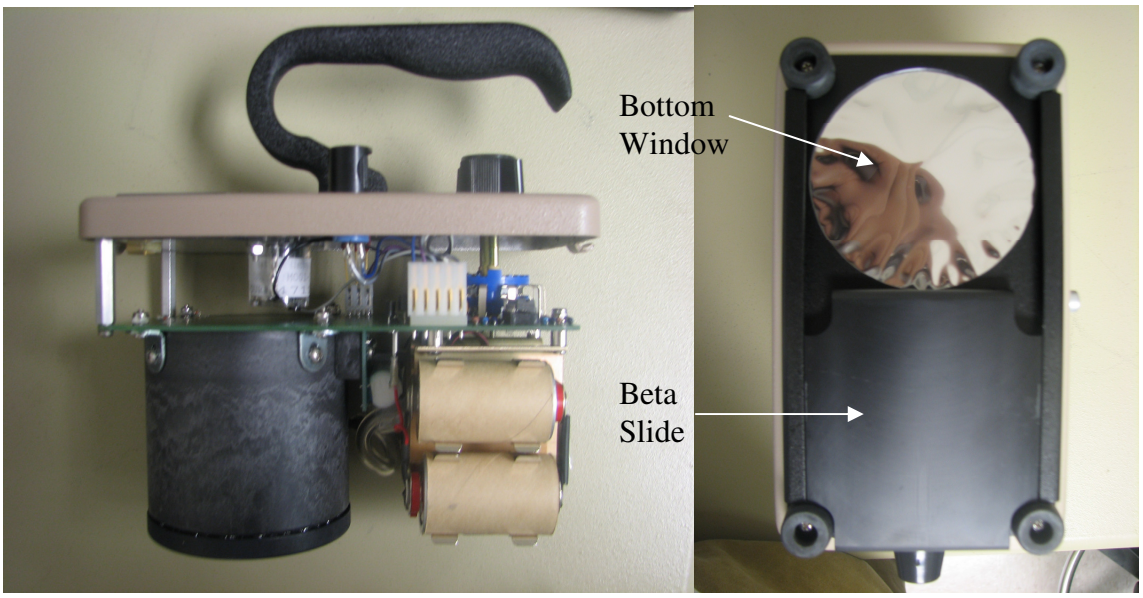

Figure 1. Side view of an Eberline RO-20 with the aluminum case removed (left). Bottom view of an Eberline RO-20 with the beta slide open showing the Mylar window (right).

The Eberline RO-7-BM, pictured in Figure 2, is also a portable ion chamber intended to measure exposure rate due to photons and beta radiation. The detector has an active volume of 7 cm^3 vented to the atmosphere. The detector is housed in a phenolic-lined aluminum case with a 7 mg/cm^2 thick Mylar beta window on the front. A Lucite cap can be affixed to the front of the instrument to provide a density thickness of 1000 mg/cm^2. This instrument is calibrated to Cesium-137 in the front, with the Lucite cap on.

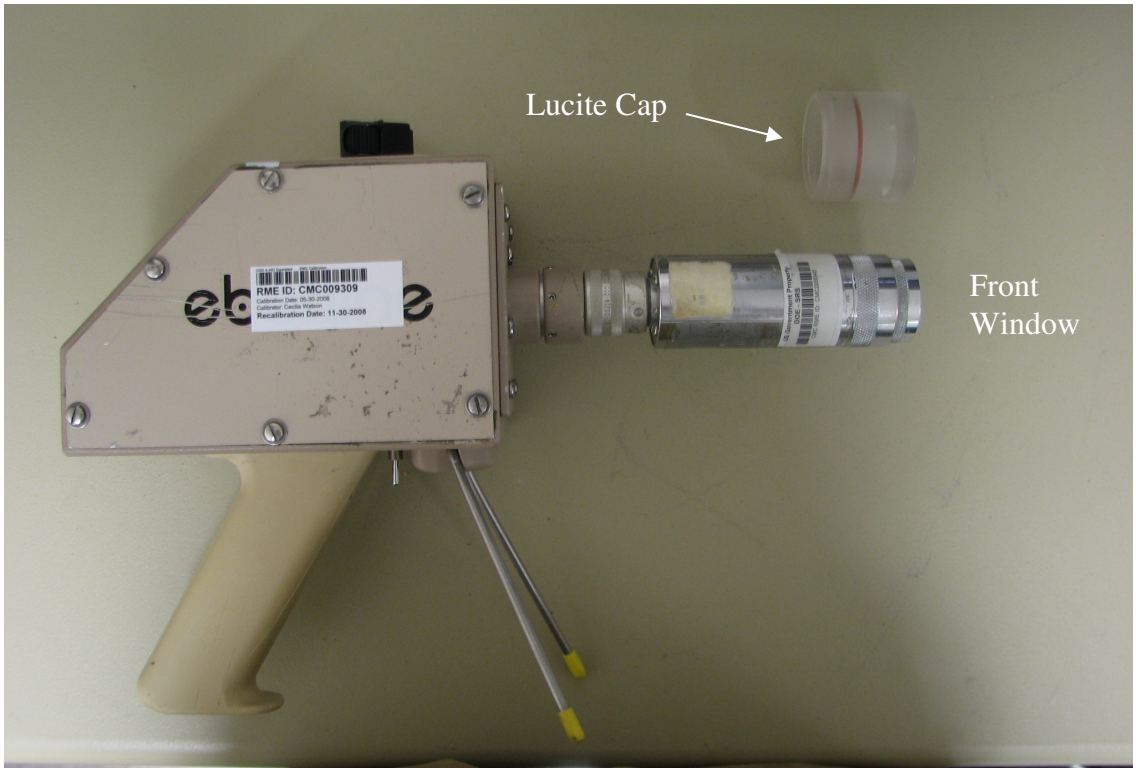

Figure 2. Side view of an Eberline RO-7-BM with the Lucite cap removed.

The Teletector 6112B, pictured in Figure 3, is a Geiger-Mueller instrument intended to measure exposure rate due to photons and beta radiation. This instrument utilizes two different Geiger-Mueller detectors, one for high and one for low-range measurements. Both detectors are sealed and filled with argon gas contained in a lead, energy-compensating case. The lead energy-compensating case, shown in Figure 3, is a hollow cylinder open on both ends. The low-range detector has an active volume of 6.3 cm^3 with a 30 mg/cm^2 mica front window. The high-range detector has an active volume of 0.1 cm^3 and is located behind the low-range detector. A rubber cap can be affixed to

the front of the low-range detector to protect the thin front window. Both detectors in this instrument are calibrated to Cesium-137 from the side, with the cap on.

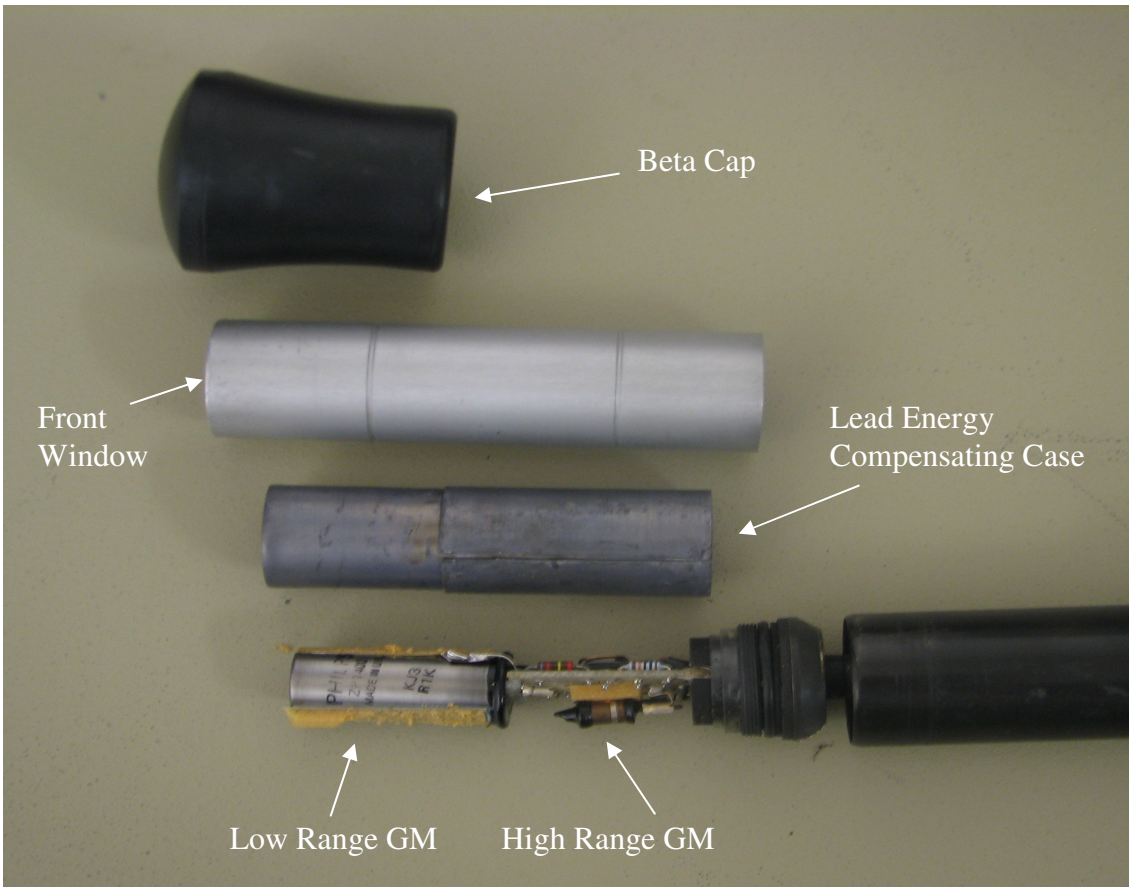

Figure 3. Disassembled view of the Teletector 6112B detector housing. Note the location of the Geiger-Mueller detectors.

The Thermo RadEye B20, pictured in Figure 4, is a pancake Geiger-Mueller instrument with many capabilities. However, this study only focused on the relative response of the instrument to photons with the available H*(10) filter. The detector is a

sealed, gas-filled pancake Geiger-Mueller with a diameter of 4.4 cm and a 2 mg/cm^2 front window. For photon measurements, an energy-compensating filter is affixed to the front of the detector. The composition and thickness of this filter are proprietary, consequently the technical specifications cannot be provided. This particular instrument measures dose equivalent rate, thus the relative response curves will be for dose equivalent rate instead of exposure rate. This instrument is calibrated to Cesium-137 in the front, H*(10) filter on configuration.

Figure 4. Front view of the Thermo RadEye B20. The H*(10) filter is not shown in this figure, but it fastens over the front window (left). Back view (right).

The Bicron Micro Rem Low-Energy, pictured in Figure 5, is a tissue-equivalent, plastic-scintillator instrument intended to measure dose equivalent rate due to photons. The detector has an active volume of 12.9 cm^3 contained in an aluminum case. The front of the instrument has a 1.3 mg/cm^2 thick window designed particularly for low-energy photons. This instrument is calibrated to Cesium-137 in the bottom configuration.

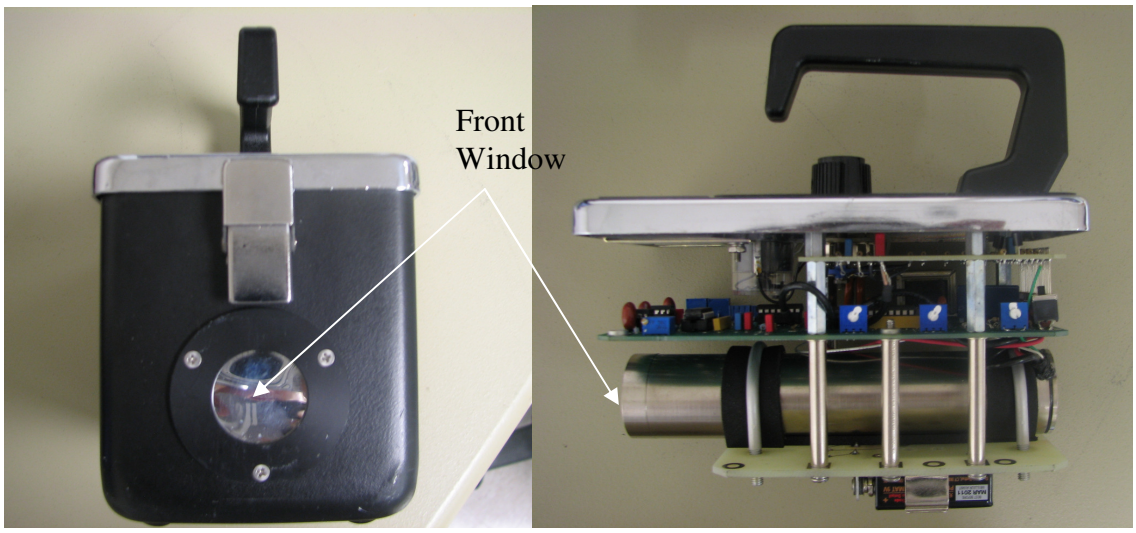

Figure 5. Front view of a Bicron Micro Rem Low-Energy. The Mylar window is characteristic of the low energy model (left). Side view with the aluminum case removed (right).

The Thermo Mk2 electronic personal dosimeter, pictured in Figure 6, is a PiN diode instrument intended to measure dose equivalent rate due to photons and beta radiation. The Mk2 has 3 PiN diode detectors connected in parallel, shielded by various thicknesses and materials. The thickness and composition of the energy compensating

case are proprietary and cannot be provided. This instrument is calibrated to Cesium-137 in the front configuration.

Table 3 provides a summary of basic characteristics and the number tested for each instrument type.

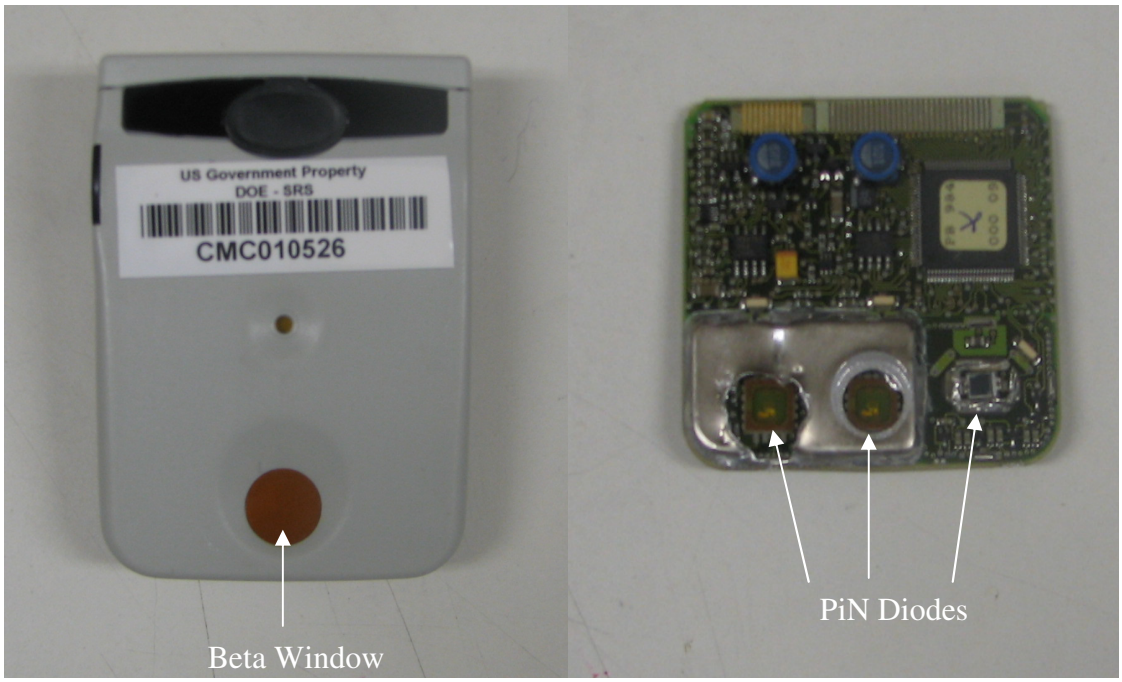

Figure 6. Front view of a Thermo MK2 electronic personal dosimeter (left). Disassembled view; the compensating case was removed on the far left diode for illustrative purposes. Note the three PiN diodes and their various shielding configurations (right).

Table 3. Instruments under investigation and their basic characteristics.

Instrument	Number Tested	Detector Type	Measured Units
Eberline RO-20	3	Vented Ion Chamber	roentgen/h
Eberline RO-7-BM	2	Vented Ion Chamber	roentgen/h
Eberline Teletector 6112B	3	2 Sealed Geiger-Mueller Tubes	roentgen/h
Thermo RadEye B20	2	Sealed Pancake Geiger-Mueller	mrem/h
Bicron Micro Rem Low Energy	3	Tissue-equivalent Plastic Scintillator	mrem/h
Thermo Mk2 Electronic Personal Dosimeter	3	3 PiN Diodes	mrem/h

The relative response of an instrument can be calculated using Equation 4. The conventionally true value of the reference photon radiation will always be the photon energy and orientation in which the instrument is calibrated (ANSI 2004). The equation is:

$$RR = \frac{\bar{r}_{en_i} / CTV_{en_i}}{\bar{r}_{ref} / CTV_{ref}} \tag{4}$$

where: RR = relative response;

$\bar{r}_{en_i}$ = mean reading of photon energy i;

$\bar{r}_{ref}$ = mean reading of reference photon radiation;

CTV_{eni} = conventionally true value of photon energy *i*; and
CTV_{ref} = conventionally true value of reference photon radiation.

C_k Dose Equivalent Conversion Factors

Generally, for photons the factor to convert from exposure to dose equivalent is assumed to be unity; however, for low-energy photons this is not the case. Some of the instruments tested in this study only measure dose equivalent rate and, since the conventionally true values are calculated in units of roentgen per hour, the results must be converted to dose equivalent rate, or rem per hour. The dose equivalent conversion factors for each source are listed in Table 4.

Table 4. C_k dose equivalent conversion factors for various sources (ANSI 2001).

Source	C_k Conversion Factor (rem/R)
H50	1.23
Am-241	1.66
H100	1.64
H150	1.50
H200	1.38
H250	1.30
H300	1.25
Cs-137	1.06
Co-60	1.03

Primary Photon Interactions

There are three major types of photon interactions; photoelectric effect, Compton scattering, and pair production. These are the primary mechanisms by which photons transfer energy to matter. Pair production is only energetically possible for photon energies greater than 1.022 MeV and since the probability for this interaction is very low even for Cobalt-60, it will be ignored. Therefore, this section will only focus on the photoelectric effect and Compton scattering interactions.

When a photon interacts with matter via photoelectric absorption, the photon energy is completely absorbed by an atom resulting in the ejection of a photoelectron with energy equal to the difference between the incident photon and the binding energy of the ejected photoelectron. The most probable electrons ejected are from the inner electron shells of the atom (K, L, and M shells). The consequential electron vacancy is promptly filled by a free electron and/or rearrangement of the electron shells producing additional photons which are absorbed close to the original atom (Attix 2004). From Figure 7, this interaction is observed to be dominant for low-energy photons and high atomic number materials.

Compton scattering occurs when a photon 'strikes' and ejects an orbital electron from an atom. The photon transfers some of its energy to the electron and is scattered at a finite angle. The orbital electron is also scattered at an angle dependent on conservation of energy and momentum (Attix 2004). For example, a photon scattering at a large angle will transfer a large portion of its energy to the recoil electron which, to

conserve energy and momentum, will scatter at a small angle. From Figure 7, this interaction is observed to be dominant for moderate energy photons.

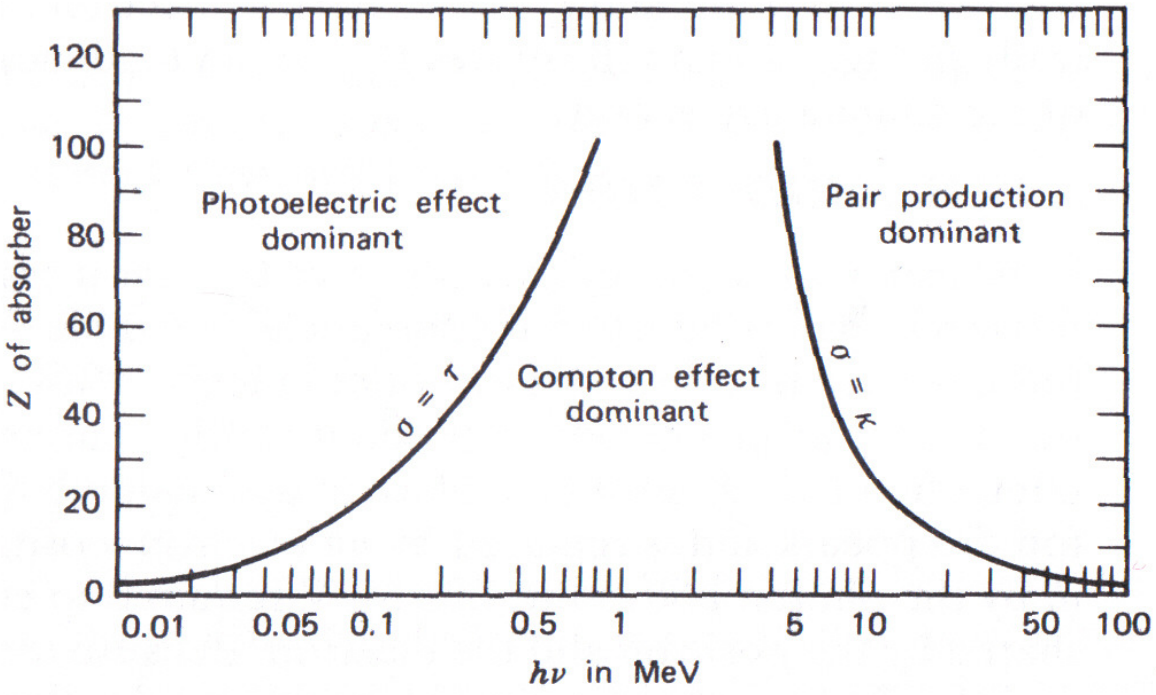

Figure 7. Relationship between Z of absorber and photon energy for the three major photon interactions (Attix 2004).

One suspected cause of instrument over and/or under-response is the variation in photoelectric and Compton scattering cross-sections. From Figure 7, it is obvious these interaction cross-sections are dependent on target material and photon energy. Plots of photoelectric and Compton scattering cross-sections for various materials commonly used in radiation instrumentation can be seen in Figures 8-10. Unlike the Compton scattering cross-section, which remains relatively constant, the photoelectric cross-

section rapidly increases by many orders of magnitude for low-energies. The increased interaction probabilities lead to higher interaction rates and may adversely affect instrument response for low-energy photons. An over response may be observed when incident photon energies are below the point where the photoelectric cross-section increases for the target material. In contrast, under responses may be observed below this point when there are additional materials between the source and detector. This decreased response is due to increased attenuation by the additional materials, reducing the number of photons and secondary electrons that reach the active volume of the detector.

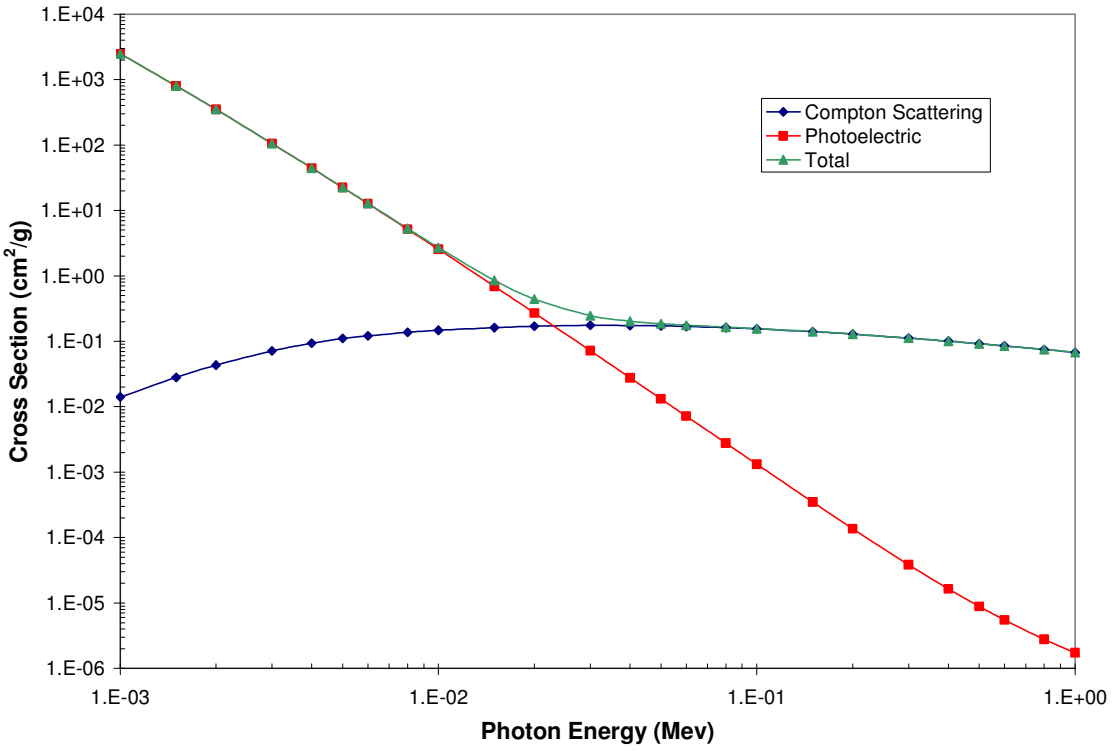

Figure 8. Photoelectric and Compton scattering cross-section vs. photon energy for Bakelite. Bakelite is an 'air equivalent' conductive plastic commonly used to construct the detector walls of an ion chamber (NIST 1998).

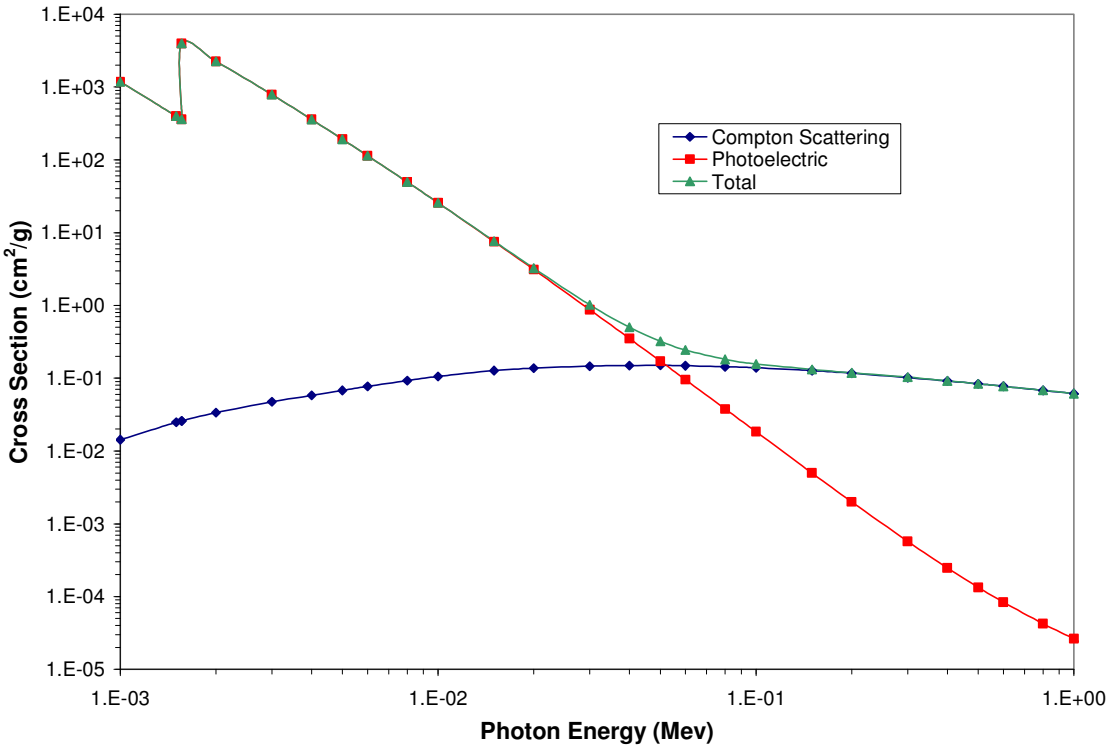

Figure 9. Photoelectric and Compton scattering cross-section vs. photon energy for Aluminum (NIST 1998).

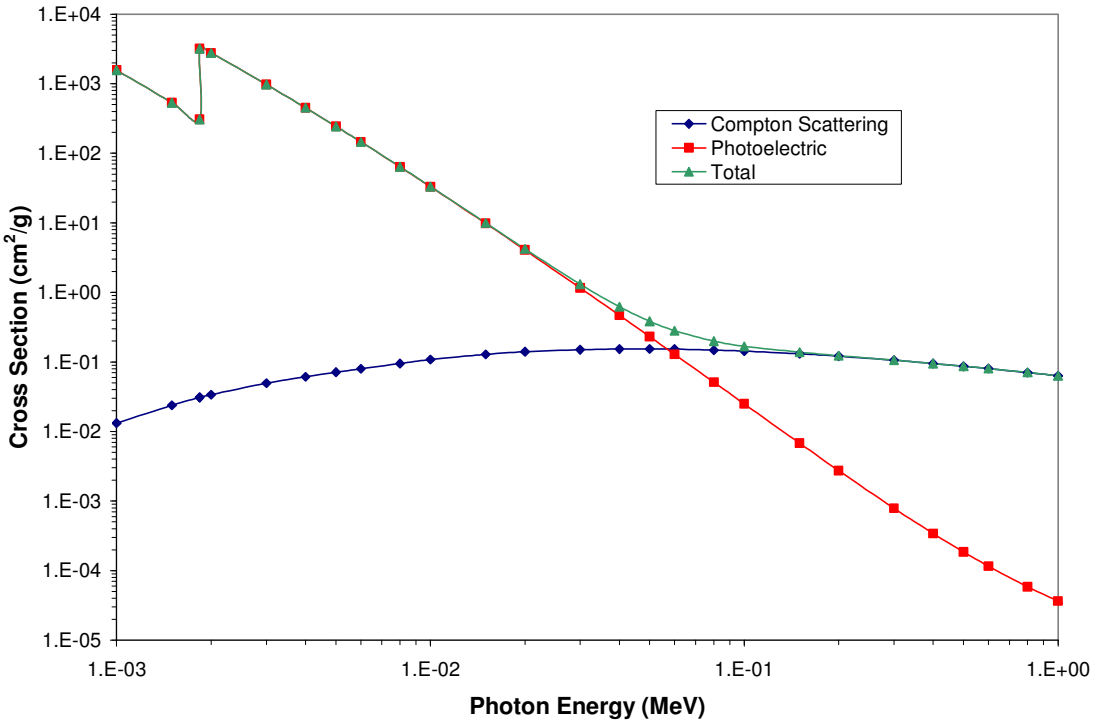

Figure 10. Photoelectric and Compton scattering cross-section vs. photon energy for Silicon (NIST 1998).

When photons traverse a medium they can undergo one or more of the interactions mentioned above. Thus, the number of photons traversing a medium can be decreased, or attenuated. The amount of attenuation is a function of the thickness of the absorber and the linear attenuation coefficient. The linear attenuation coefficient is the sum of all the interaction cross-sections. Equation 5 can be used to calculate the photon intensity emitted from a source after traversing a medium (Attix 2004):

$$I = I_0 e^{-\mu t} \tag{5}$$

where: I_0 = initial intensity;

μ = linear attenuation coefficient; and

t = thickness of absorber.

CHAPTER III

MATERIALS AND METHODS

Measurement and Calculation of Conventionally True Values

An Exradin A4 ion chamber was centered at a fixed distance of 100 cm from the x-ray tube and connected to a Keithley Model 6517 electrometer which supplied -500 V to the ion chamber. The ion chamber and electrometer setup were allowed to stabilize for 15 minutes, thereafter, 10 leakage current measurements were recorded and averaged. Before any calibration measurements were taken, the room temperature and atmospheric pressure were measured, recorded, and substituted into Equation 2 to calculate the temperature and pressure correction factor. The ion chamber was exposed to radiation and the electrometer was utilized to measure the electrical charge per unit time (electrical current) created by ionizing radiation incident in the ion chamber. Measurements of electric current generated in the ion chamber were recorded in 2 mA increments of current applied to the x-ray tube. The measured current and temperature and pressure correction factor were substituted into Equation 3 to calculate the exposure rate at each measurement point. A plot of exposure rate vs. x-ray tube current was constructed and a linear trend line was fit to the data. This entire process was repeated for every beam code listed in Table 2.

Since the lowest exposure rates from the x-ray irradiator at 100 cm exceed the maximum range of the Bicron Micro Rem LE, supplementary measurements were made.

Using the same method previously mentioned exposure rates were calculated at single values of applied tube current, 250 cm from the source for each beam code.

For the Americium-241 source, a similar procedure was followed with the exception of the following. Measurements of electric current were made in 5 cm increments from 30-100 cm (with the exception of 80, 90, and 95 cm) along the centerline of the beam on the x-axis. Since the National Institute of Standards and Technology does not calibrate ion chambers for the gamma-ray emitted from Americium-241, a calibration factor was obtained by interpolation between values for the H50 and H100 beam codes. This was done by plotting the calibration coefficients for each beam code listed in Table 2 vs. their respective effective energies. Again, Equations 1-3 were used to calculate the exposure rate at each measurement point. A plot of exposure rate vs. distance was constructed and an exponential trend line was fit to the data. The conventionally true values for the Cesium-137 and Cobalt-60 sources were obtained through existing calibration records.

Determining Relative Response

Exposure rates for each instrument, at each energy, were appropriately chosen so that the anticipated measured exposure rate fell in the middle of the detector range. With the detector centered along the x-axis of each beam, every instrument was exposed to all of the sources listed in Table 1 in various configurations. Generally the configurations included exposure to the front, side, and bottom of the instrument. If a beta cap or slide was a feature of the detector, configurations with and without the beta cap were also

investigated. The exposure rate measured by the instrument was recorded, and an average for each energy, in each orientation was computed. In the cases where the instrument measured dose equivalent rate, the conventionally true exposure rates were converted to dose equivalent rate using the C_k factors listed in Table 4. The conventionally true value of the reference radiation is dependent on the instrument type and is deemed to be the energy and orientation in which that specific instrument is calibrated. The measured and conventionally true values were substituted into Equation 4 to calculate the relative response. A plot of relative response vs. effective photon energy was constructed for each instrument type, including response curves corresponding to each orientation.

Based on the relative response curves, an ideal orientation was chosen for each instrument. If the ideal orientation had relative responses > $\pm$20% (ANSI 2004), correction factors were calculated to obtain a relative response of ~1. The potential sources of the under and/or over-responses were analyzed for each instrument.

CHAPTER IV

RESULTS AND DISCUSSION

Conventionally True Exposure Rates

By substituting the measured electric current from the ion chamber/electrometer setup and the ambient temperature and pressure into Equations 1-3, the conventionally true exposure rates for each beam code were calculated. These exposure rates were plotted vs. x-ray tube current for each beam code and are shown in Figures 11-16. Since the current applied to the x-ray tube is directly proportional to the quantity of x-rays produced, a linear trend line was fit to each plot. Each plot yielded a regression coefficient ≥ 0.9995, indicating a near perfect linear line. The small variations obtained for the regression coefficient may be attributed to slight non-linearity of the current meter used to adjust the current applied to the x-ray tube. The equation of the trend line and the corresponding regression coefficient can be seen on each plot. In some circumstances, the equation of the line was used to calculate any conventionally true exposure rates lying between data points.

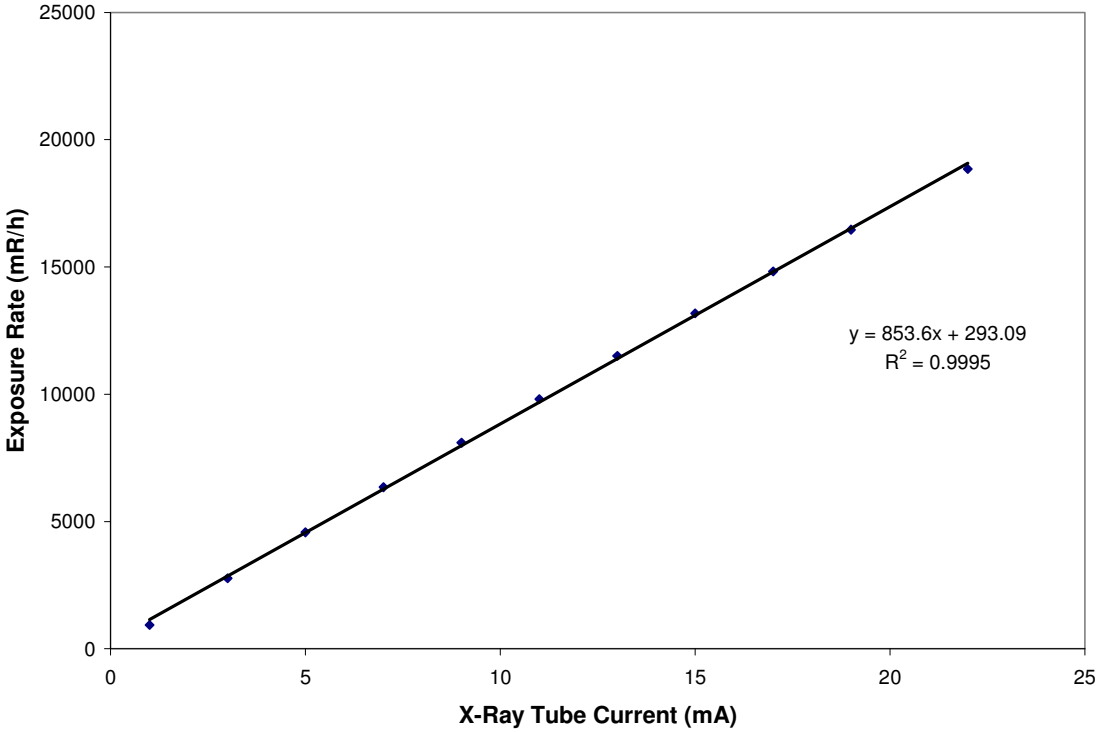

Figure 11. Conventionally true exposure rates for the H50 x-ray beam code.

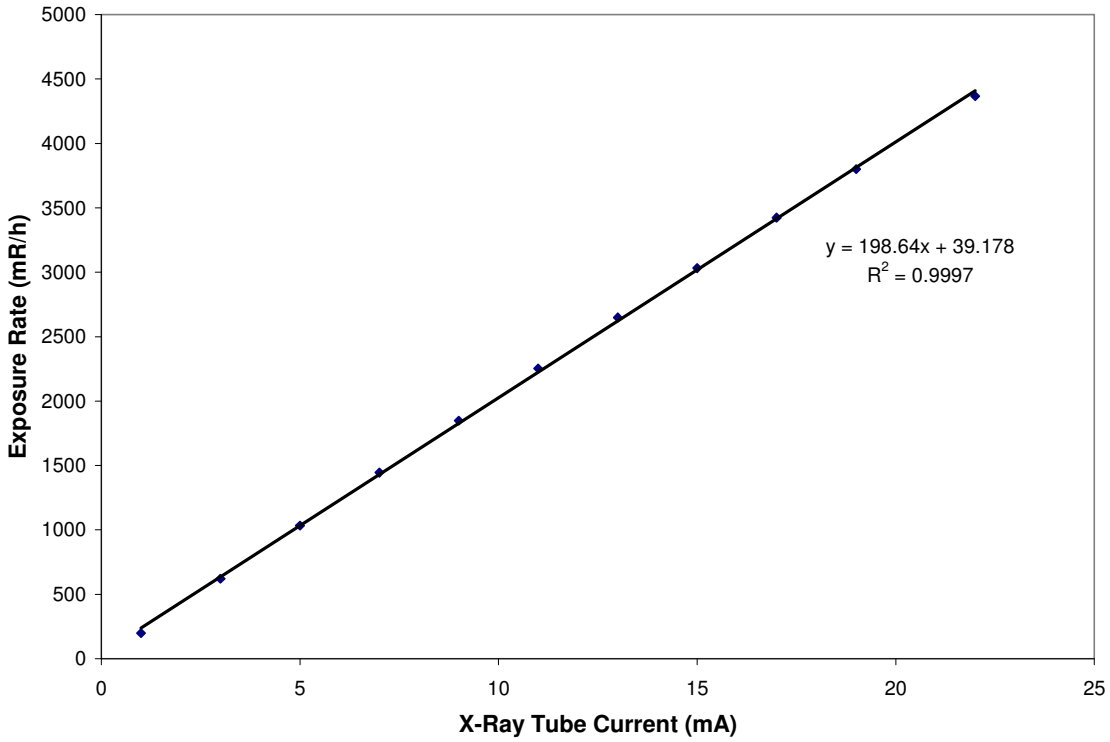

Figure 12. Conventionally true exposure rates for the H100 x-ray beam code.

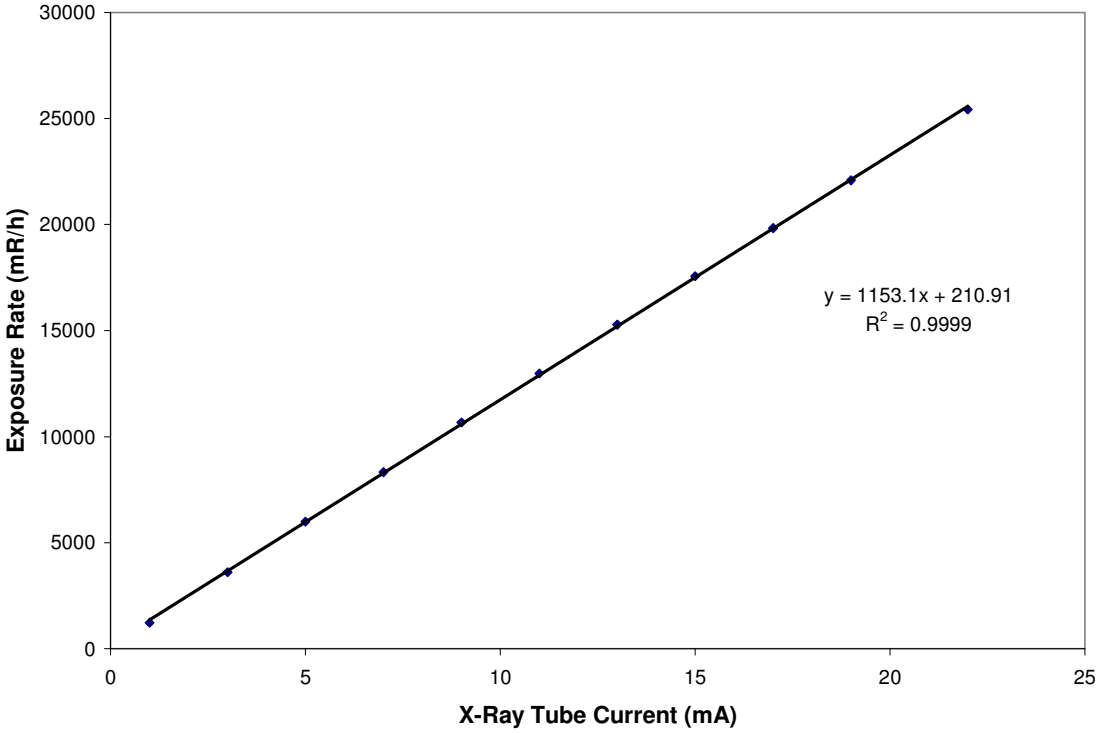

Figure 13. Conventionally true exposure rates for the H150 x-ray beam code.

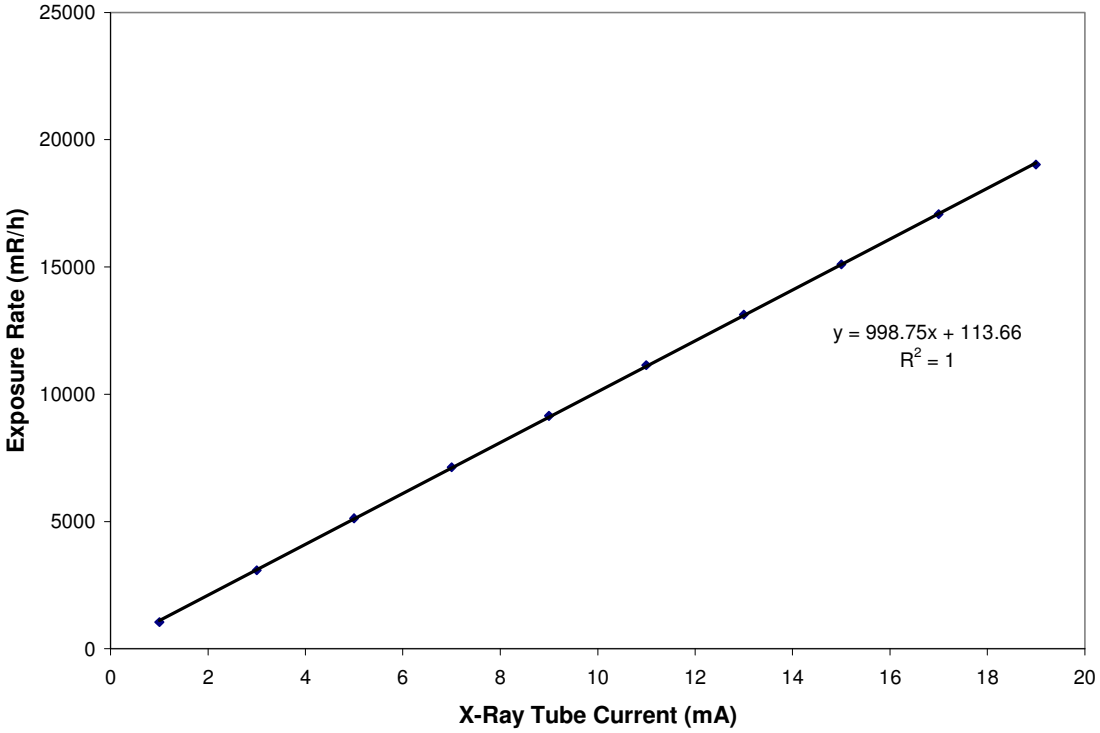

Figure 14. Conventionally true exposure rates for the H200 x-ray beam code.

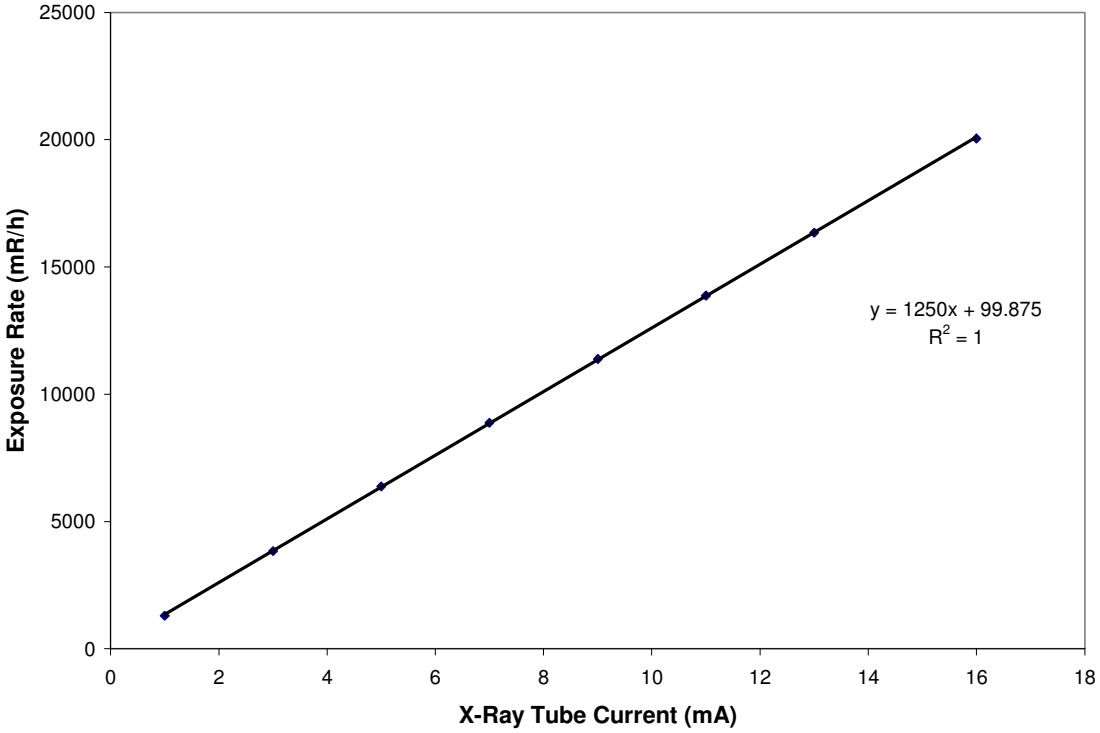

Figure 15. Conventionally true exposure rates for the H250 x-ray beam code.

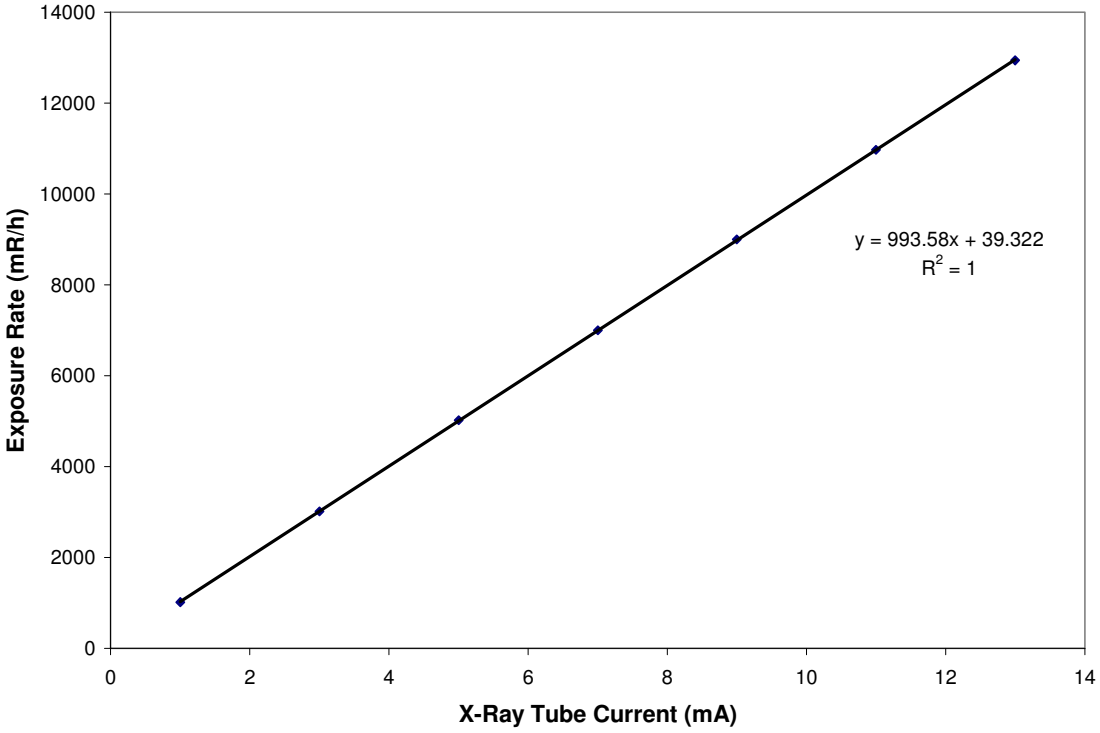

Figure 16. Conventionally true exposure rates for the H300 x-ray beam code.

The Bicron Micro Rem LE has a much lower measurement range than the other instruments in this study. Consequently, additional measurements were made at 250 cm from the source with very low current applied to the x-ray tube. These additional measurements were made using the same method and equations as previously mentioned. The conventionally true values, listed in Table 5, were used only for the Bicron Micro Rem LE.

Table 5. Conventionally true exposure rates at 250 cm from the x-ray source.

Beam Code	Applied X-ray Tube Current (mA)	Calculated Exposure Rate (mR/h)
H50	0.5	69
H100	2.0	77
H150	0.5	100
H200	0.5	85
H250	0.5	108
H300	0.5	87

From Figure 17, a plot of calibration factor vs. effective energy, a calibration factor of 1.0554E+6 was interpolated for Americium-241. This value along with the electric current measured by the ion chamber/electrometer setup was substituted into Equation 3 to calculate the conventionally true exposure rates for Americium-241. Figure 18 shows the exponential relationship between exposure rate and distance from the source. An exponential trend line was fit to the data yielding a regression coefficient

of 0.9997. The equation of the line was used to calculate conventionally true exposure rates that lie between data points.

The slight variations in Figure 17 may be attributed to the difference in homogeneity coefficient for each beam code. A smaller homogeneity coefficient means the beam code has a 'softer' spectrum; consequently there are more low-energy photons present in the spectrum compared to a beam code with a higher homogeneity coefficient. For example, the H50 beam code has a homogeneity coefficient of 93% and the H300 beam code has a homogeneity coefficient of 99%. Thus, the H300 beam code has a 'harder' or more monoenergetic photon spectrum.

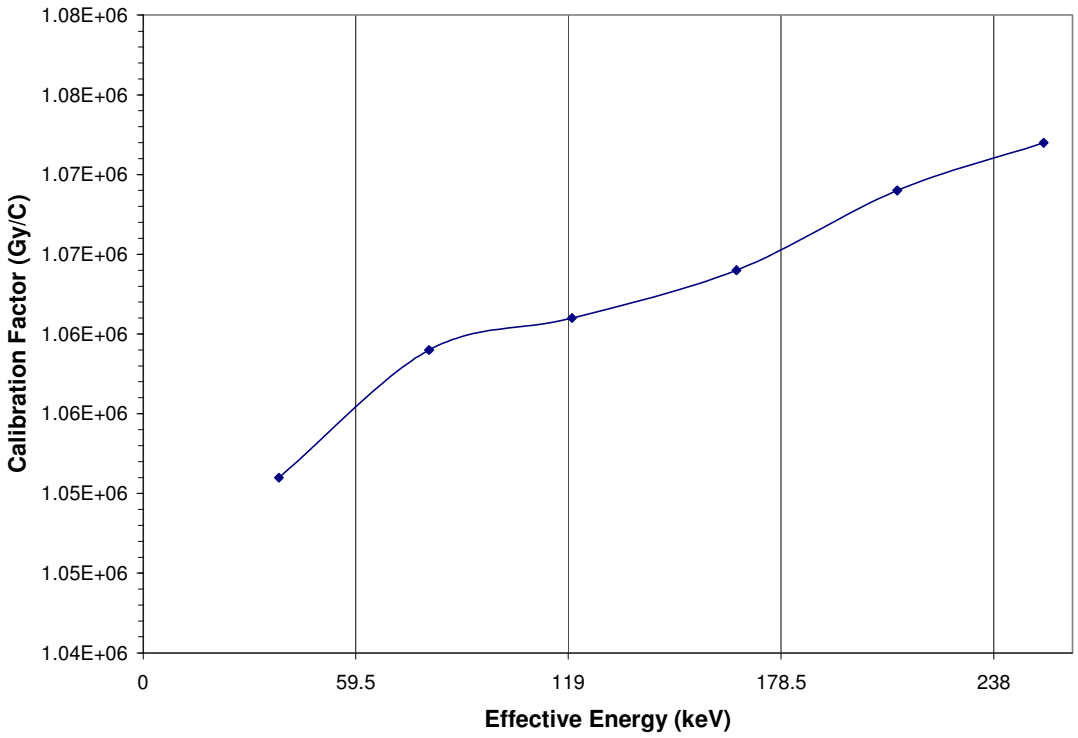

Figure 17. Calibration factor vs. effective energy for Exradin A4 ion chamber.

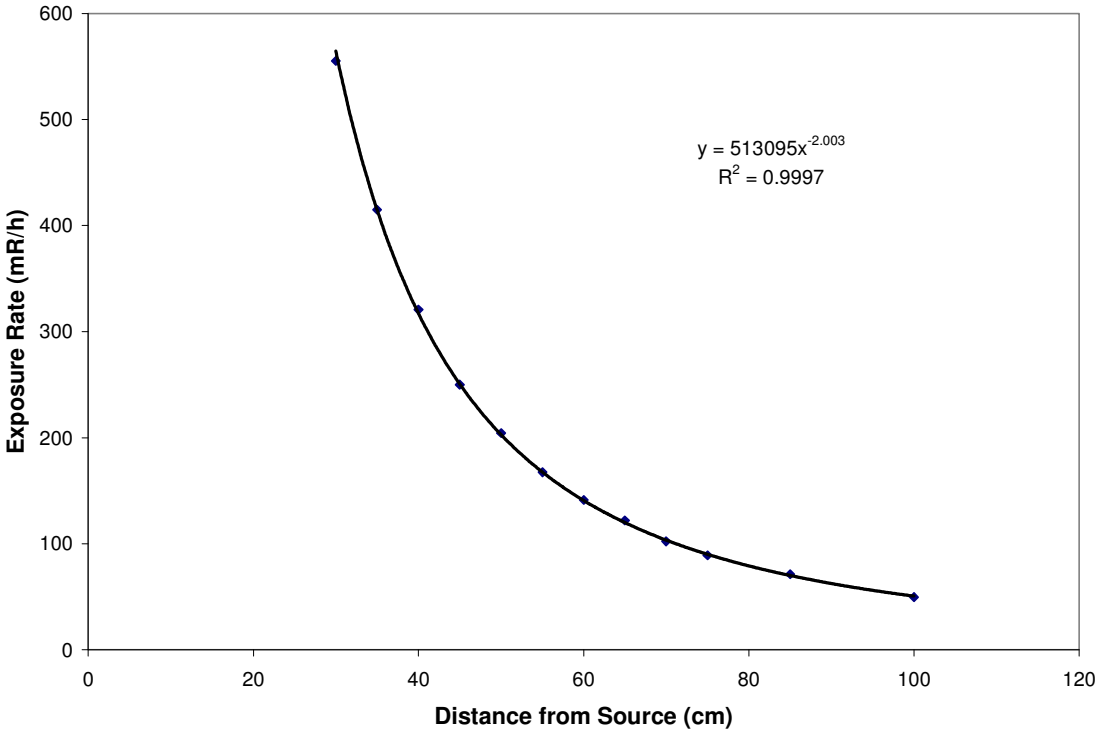

Figure 18. Conventionally true exposure rate vs. distance for Americium-241.

Instrument Relative Response Plots

Each instrument was exposed to all of the sources listed in Table 1. To calculate the relative response for each instrument type, the measured exposure rate at each energy and orientation were averaged and substituted into Equation 4 along with the analogous conventionally true exposure rate. For instruments that measure dose equivalent rate, the measured and conventionally true exposure rates were converted to dose equivalent rate using the factors listed in Table 4. The relative response plots for each instrument

type can be seen in the following figures. Using these plots an ideal orientation was chosen and if responses were > ±20%, correction factors were determined.

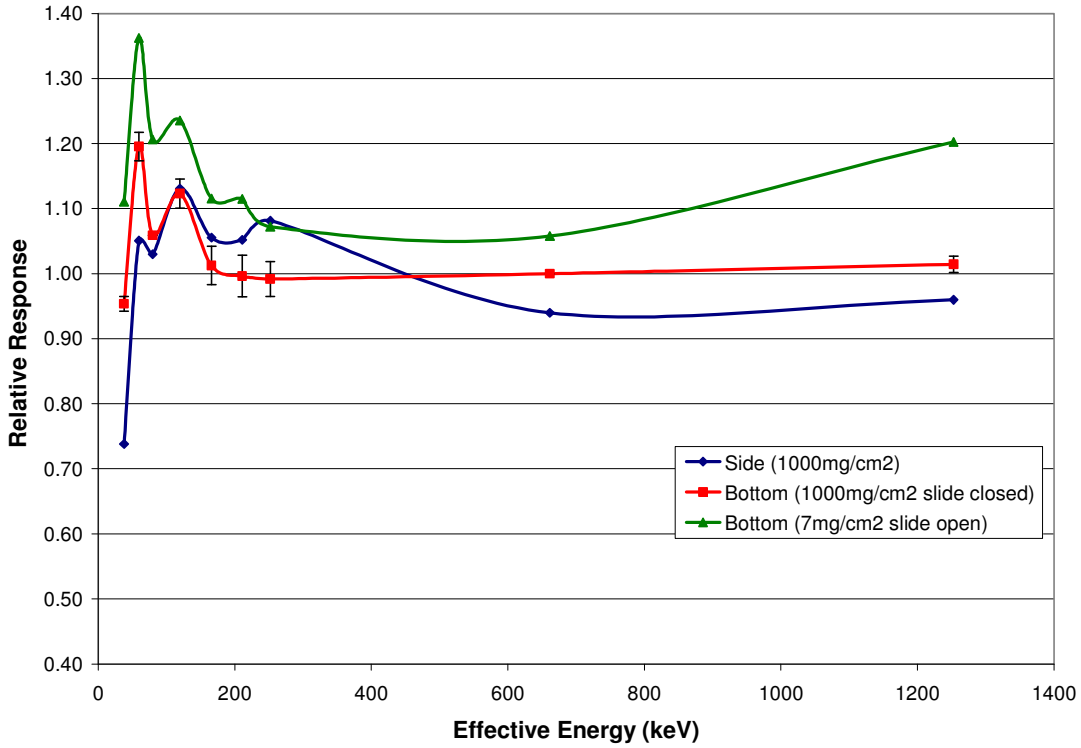

Figure 19. RO-20 relative response curves. All curves relative to Cs-137 bottom, slide closed.

Based on Figure 19, the ideal orientation for the RO-20 was chosen to be the bottom with the beta slide closed. Since the responses for the entire photon energy range in this orientation are within ± 20%, no correction factors were necessary. The slight over responses below ~120 keV are a combination of the increasing photoelectric cross-section and the range of secondary electrons in air and the beta slide. At these energies,

the range of secondary electrons created in the beta slide becomes comparable to the dimensions of the detector, resulting in more energy deposition in the active volume (Chang-ming and Nahum 1991). A maximum is observed at ~60 keV, thereafter the curve decreases due to attenuation from the beta slide. Since the photoelectric cross-section sharply increases as photon energy decreases, one may expect the relative response to also increase. However, below 60 keV the range of photoelectrons created in the beta slide is not sufficient to reach the active volume. Attix (2004) reports comparable characteristics of this response curve with a graph of typical energy-dependence per unit exposure for health physics instrumentation.

The bottom, slide open configuration follows the same trend as the slide closed configuration. In the absence of the beta slide, there is less attenuating material between the source and detector resulting in a higher response, shifting the entire curve up. The side response curve also follows the same general trend, except below 60 keV. This variation can be attributed to the difference in materials with the side orientation. In the bottom orientation, photons pass through the beta slide and a very thin Mylar window before entering the active volume; however in the side orientation, they must pass through the aluminum case, a small air gap, and the detector wall before entering the active volume. For photons below 60 keV the total attenuation cross-section increases rapidly, due to the onset of photoelectric effect, reducing the number of subsequent electrons reaching the active volume. While the density thickness for the side and bottom orientations are roughly the same, the range of secondary electrons created by interactions in the aluminum case prevents many of them from passing through the wall

of the detector. Similar response curves for ion chamber instruments have been observed by Storm et al (1974).

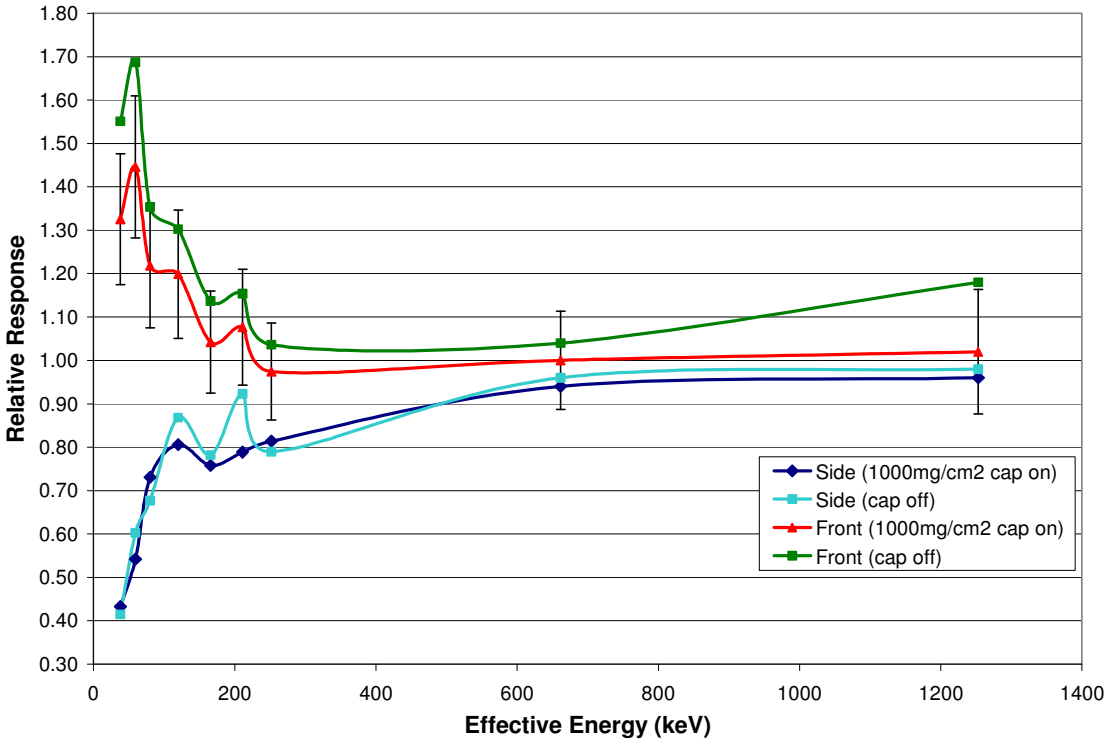

Figure 20. RO-7-BM mid range relative response curves. All curves relative to Cs-137 front, cap on.

Based on Figure 20, the ideal configuration for the RO-7-BM was chosen to be the front with the beta cap on orientation. For energies below 120 keV a correction factor of 0.8 can be applied to achieve more accurate measurements. Like the RO-20, over responses are observed below ~120 keV increasing to a maximum at 60 keV, followed by a decrease. The front cap on/off curves follow the same trend, again with

the cap off there is less material providing attenuation resulting in a higher response and shifting the curve up. The side cap on/off curves virtually lie atop one another with a similar attenuation effect to the RO-20 below photon energies of 80 keV. The Lucite cap does not appear to have a significant effect on the relative response in the side orientation.

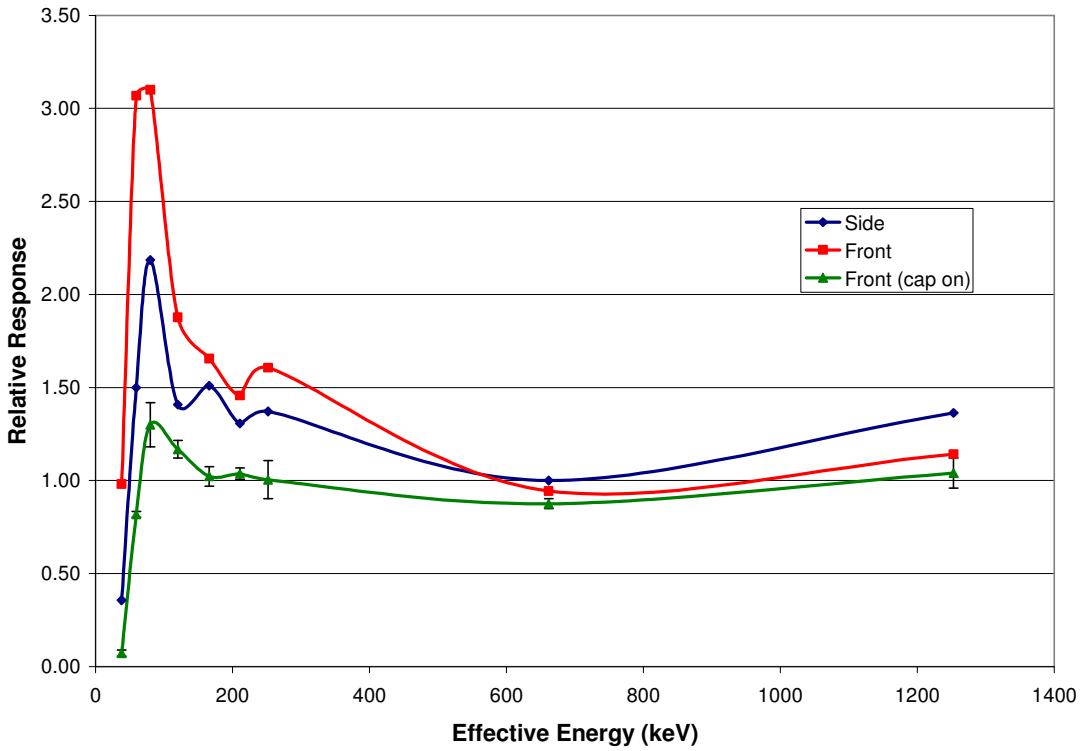

Figure 21. Low range Teletector relative response. All curves relative to Cs-137, side.

Based on Figure 21, the ideal configuration chosen for the low-range scale on the Teletector is the front with the cap on. In this orientation, a correction factor of 0.7 should be used for energies between 80 - 120 keV. The other orientations follow the

same trends; however enormous over responses are observed for energies between 60 - 252 keV. These large over responses are characteristic of Geiger-Mueller detectors, which cannot discriminate photon energy (Knoll 2000). The photoelectric cross section for argon (the detector fill gas) rapidly increases below 100 keV, therefore the probability of interaction also increases. Since a single interaction produces an electrical signal, an increased interaction rate results in a larger number of pulses measured, leading to the dramatic over response. In the absence of the beta cap, this characteristic is amplified due to the lack of attenuation material.

Also, in some cases, this instrument severely under responds, therefore it should not be used for energies below 59 keV in the front, cap on and side orientations. The under response is a result of severe attenuation from the beta cap and the energy compensating case. However, if the cap is removed, reducing the amount of attenuation, this instrument can be used to measure 38 keV photons accurately. Similar response curves for Geiger-Mueller instruments have been observed by Storm et al (1974).

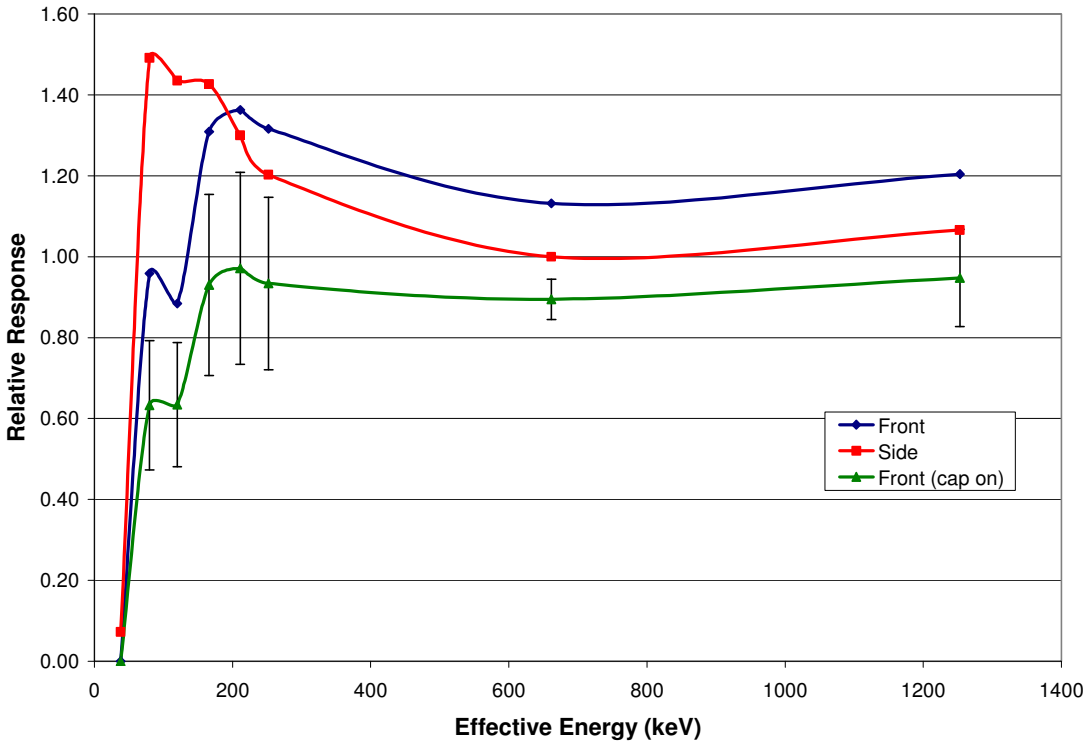

Figure 22. High range Teletector relative response. All curves relative to Cs-137, side. The Americium-241 response is not included in this plot due to its relatively low source strength compared to the instruments measurement range.

Based on Figure 22, the ideal configuration chosen for the high-range scale on the Teletector is the front with the cap on. In this orientation, a correction factor of 1.5 should be used for energies between 80 - 120 keV. Like the low-range detector, the over responses are due to the increasing photoelectric cross-section for Argon. On the other hand, the over responses are smaller in magnitude compared to the low-range detector. This can be attributed to the size and location of the high-range detector. The high-range detector has a much smaller active volume, reducing its sensitivity. Also, it is situated behind the low-range detector. In the front configuration, photons must pass through the

low-range detector and the associated electronics before being detected in the high-range detector. These additional materials decrease the photon intensity and consequently decrease the interaction rate within the active volume yielding a lower response.

Also, in some cases, this instrument severely under responds, therefore it should not be used for energies below 80 keV in the front, cap on and side configurations. However, if the cap is removed, reducing the amount of attenuation, this instrument can be used to measure 80 keV photons accurately. The Americium-241 source strength is very low compared to the measurement range of the high-range detector; consequently this photon energy could not be included in Figure 22.

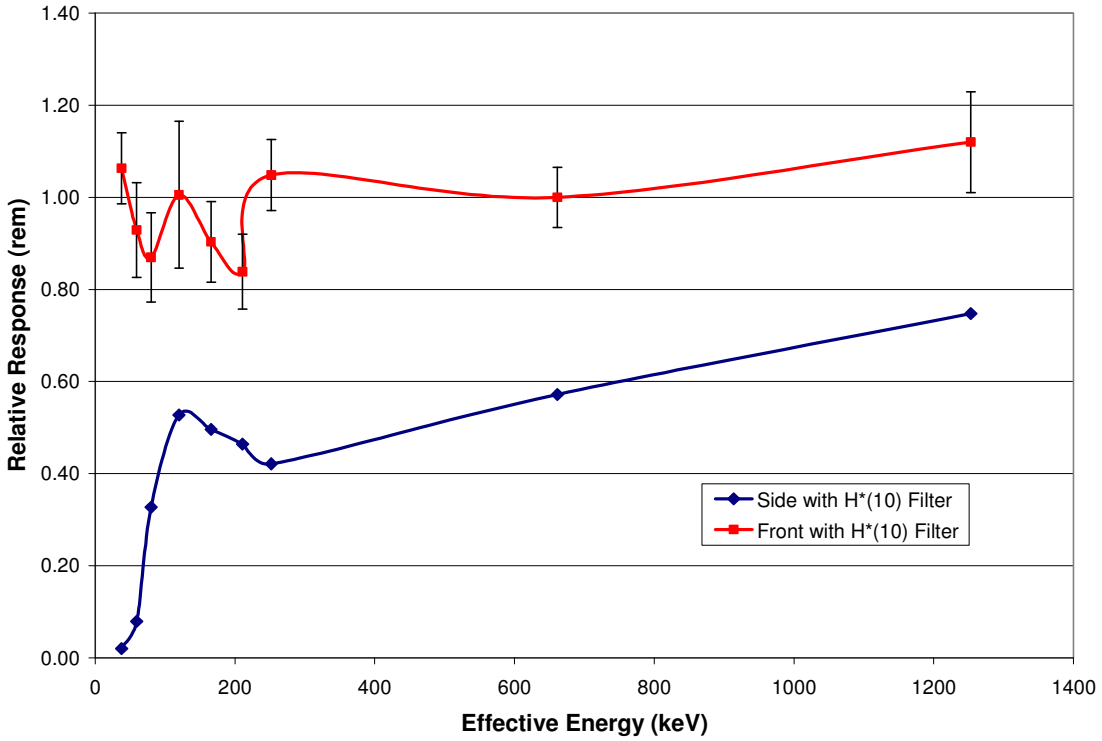

Figure 23. RadEye B20 relative response. All curves relative to Cs-137, front with H*(10) filter.

Based on Figure 23, the ideal configuration chosen for the RadEye B20 is the front with the H*(10) filter. Since the response in this orientation is within $\pm$ 20% over the entire energy range, no correction factors are necessary. Unlike the Teletector, no significant under or over responses are observed with the RadEye B20. This is likely a characteristic of the proprietary H*(10) filter, which appears to be a combination of various materials appropriately chosen to alter the photon spectrum below 300 keV. The large under response for the side configuration is due to the detector geometry. The H*(10) filter only covers the front face of the detector and is not designed to be used in

the side configuration. Also, this is a pancake detector, making it very angular dependent due to the changing cross-sectional area of the detector with respect to incident angle.

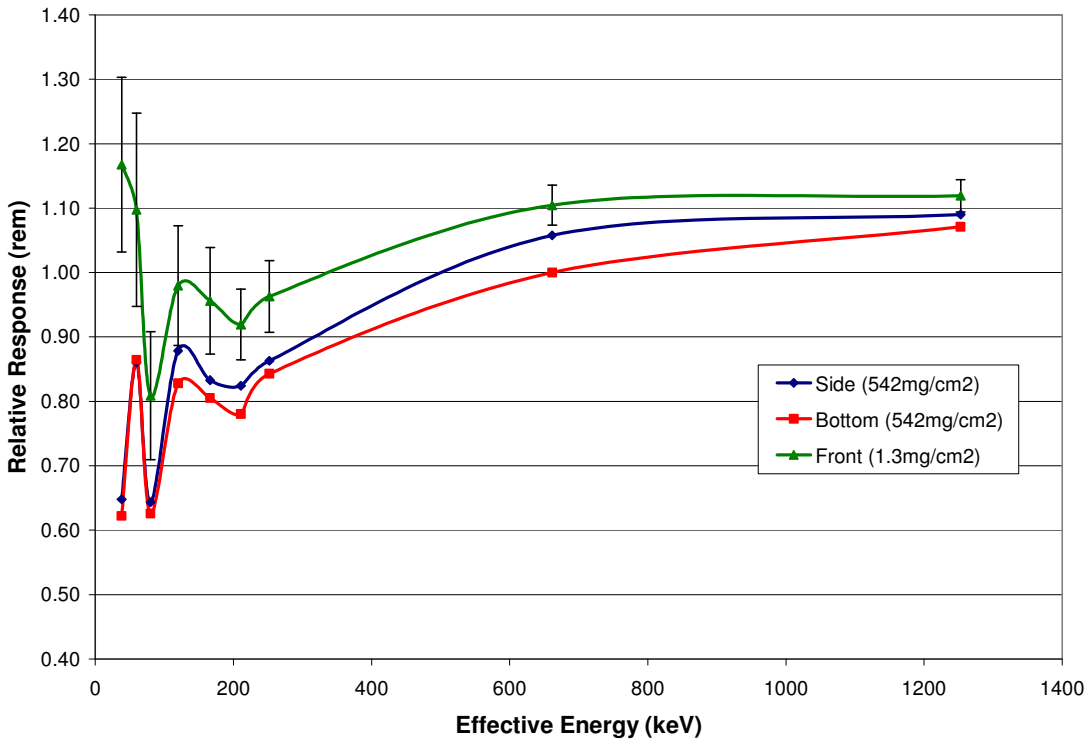

Figure 24. Bicron Micro Rem LE relative response. All curves relative to Cs-137, bottom.

Based on Figure 24, the ideal orientation chosen for the Bicron Micro Rem LE is the front configuration. This instrument is specifically designed for low-energy photons and since the response in the ideal orientation is within $\pm$ 20% over the entire range, no correction factors are needed. The thin window allows more low-energy photons to reach the active volume of the detector, increasing the sensitivity. The other two

orientations follow this same general trend except for the lowest energy. Both curves show a lower response, due to the added attenuation from the aluminum case, shifting the curves down. The effect of attenuation is amplified for lower-energy photons due to the drastic increase in photoelectric cross-section for aluminum.

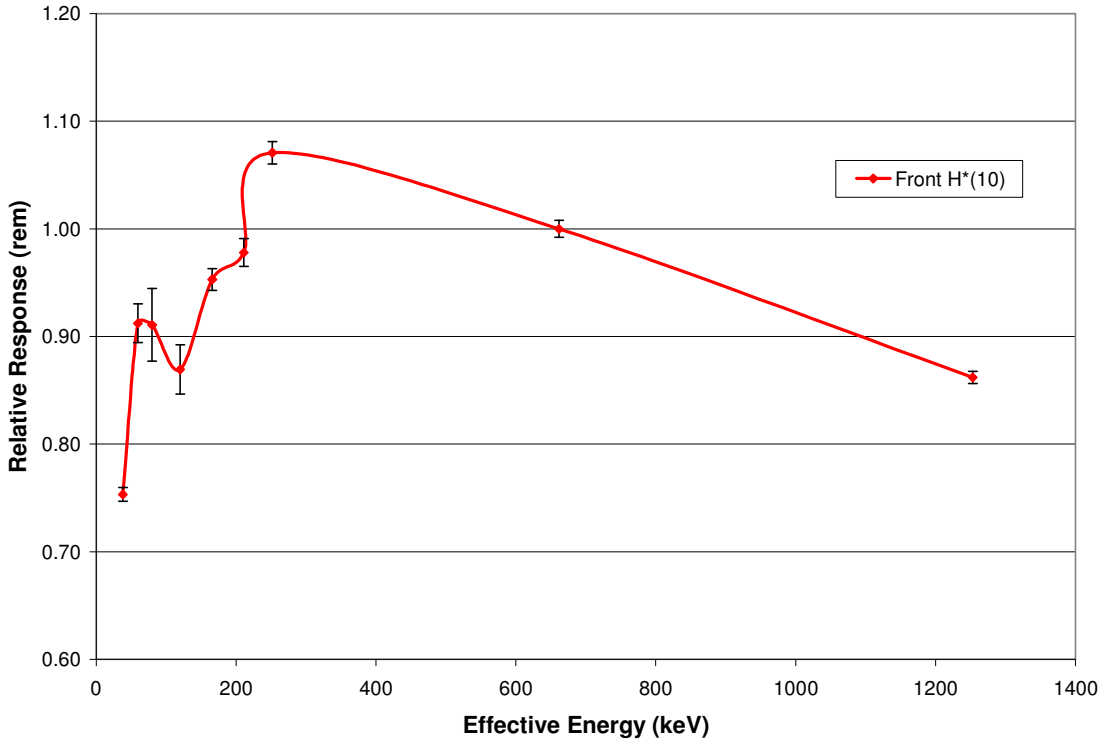

Figure 25. Mk2 EPD relative response relative to Cs-137.

The Mk2 EPD is worn on an individual in only one orientation, thus this is the ideal configuration. Based on Figure 25, a correction factor of 1.25 should be applied for photons below ~40 keV to accurately measure dose equivalent rate. Generally the response of silicon diode detectors increases significantly for photon energies below 300

keV (Olsher and Eisen 1996). However, like Geiger-Muller detectors, energy compensating filters can be used to attenuate and effectively flatten the energy response. In this case, an energy compensating filter combined with multiple silicon diodes nearly flattens the energy response, except below 40 keV. At this point, the energy compensating filter begins to drastically reduce the number of secondary electrons that reach the active volume of the diode. Similar response curves have been observed by others using single PiN diodes shielded by various materials (Olsher and Eisen 1996).

CHAPTER V

CONCLUSION

The results indicate that instrument orientation and photon energy are important factors when trying to accurately measure exposure or dose equivalent rate. An ideal configuration for each instrument was chosen and correction factors were determined for photon energies with a relative response greater than $\pm$ 20%. The ideal configuration and corresponding correction factors for each instrument are listed in Table 6. Window attenuation, varying interaction cross-sections, and the range of secondary electrons were found to be the primary causes of under or over response.

Table 6. Summary table of ideal configurations and correction factors.

Instrument	Ideal Configuration	Correction Factor
Eberline RO-20	Bottom, beta slide closed	None
Eberline RO-7-BM	Front, beta cap on	0.8 below 120 keV
Eberline Teletector 6112B (low range)	Front, cap on	0.7 for 80 - 120 keV Not suitable below 59 keV*
Eberline Teletector 6112B (high range)	Front, cap on	1.5 for 80 - 120 keV Not suitable below 80 keV*
Thermo RadEye B20	Front with H*(10) filter	None
Bicron Micro Rem Low Energy	Front	None
Thermo Mk2 EPD	Front	1.25 below 40 keV

*With the beta cap removed relative response ~1.

For instruments with a beta attenuator and/or the detector housed in an aluminum case, photoelectric absorption and the range of the subsequent photoelectrons were found to be the main causes of under or over response. In orientations in which photons must pass through the aluminum case, the photoelectric cross-section sharply increases below 100 keV limiting the quantity of photoelectrons that ultimately reach the active volume, resulting in a decreased response. Comparing configurations in which a beta attenuator is on or off, an increased response was observed without the attenuator due to the lack of material available for interaction. This was observed for the RO-20, RO-7-BM, and Bicron Micro Rem LE. Additionally, for energies below ~120 keV incident on ion chamber instruments, the range of secondary electrons becomes comparable to the dimensions of the detector. As a result, more energy is deposited leading to an increased response reaching a maximum at ~60 keV, thereafter the response declines due to window attenuation.

Argon is the primary fill gas for Geiger-Mueller detectors and since these detectors only rely on a single interaction to produce an electric signal, an increased interaction rate (due to the steep increase in photoelectric cross-section for argon) produced significant over responses in the Teletector 6112B. A common method to combat this effect is to enclose the detector in an energy compensating case. For the RadEye B20 and the Mk2 EPD this proved to be effective, producing fairly flat response curves.

It is important to note that in certain situations angular dependence can also be an important factor. For photon energies below 300 keV, the high and low-range Teletector

will over respond if the correction factors are applied and the detector is being exposed in the front and side orientations simultaneously (e.g, a line source). This effect may not be as severe for the high-range detector if the correction factor is not applied. Additionally, the pancake style detector of the RadEye B20 is inherently angular dependent. At incident angles greater than ~$\pm$45° the instrument will drastically under respond and yield erroneous measurements.

It is also important to note that in certain situations the error associated with an instruments relative response must be considered. Although the average relative response may be less than $\pm$20%, if the error bars are large, the relative response can extend to values greater than $\pm$20%. For example, in the ideal orientation, the average relative response of the Bicron Micro Rem LE is within $\pm$20%, however, below 80 keV the error bars extend beyond $\pm$20%. Thus, an over response may be observed at photon energies below 80 keV.

Based on these results, it is important for the user to be aware of the relative response for the configuration which the instrument is being used. Of equal importance is to ensure the measureable photon energy range of the instrument is suitable for the source term. It is important to note that if the source term is unknown or if the source emits a wide range of photon energies, the correction factors are irrelevant. For this case an energy independent instrument should be utilized. Also, all of these instruments were calibrated using Cesium-137 in a specific orientation. The relative response curves can purposely be altered by calibrations with a different sources and/or orientations. Hence,

facilities that have a wide range of source terms can calibrate a set of instruments for specific applications.

One possible improvement to this research includes using various radioisotopes with photon energies from 30 keV to 650 keV. Unlike radioisotopes, x-ray beam codes do not yield perfectly monoenergetic photons. Because of this, photons emitted by radioisotopes may provide a better representation of an instruments relative response. Also, further investigation of the instruments response to different source geometries is of interest. The photon sources used in this study were directional beams. If the instrument was exposed to a line source or two different sources so that the instrument is exposed in a front and side orientation, the relative response may change significantly. Both of these improvements more accurately mimic conditions that are commonly encountered during field measurements.

REFERENCES

American National Standards Institute. N42.17A-2003. Performance Specifications for Health Physics Instrumentation – Portable Instrumentation for Use in Normal Environmental Conditions. New York, NY: The Institute of Electrical and Electronics Engineers; 2004.

American National Standards Institute. N13.11-2001. Personnel Dosimetry Performance Criteria for Testing. McLean, VA: Health Physics Society; 2001.

Attix F. Introduction to Radiological Physics and Radiation Dosimetry. Weinheim, Germany: WILEY-VCH Verlag GmbH & Co. KGaA; 2004.

Chang-ming M, Nahum A. Bragg-Gray Theory and Ion Chamber Dosimetry for Photon Beams. Physics in Medicine and Biology. 36(4):413-428; 1991.

Knoll G. Radiation Detection and Measurement. 3rd ed. Hoboken, NJ: John Wiley & Sons, Inc; 2000.

National Institute of Standards and Technology. XCOM: Photon Cross Sections Database. Available at: http://www.nist.gov/physlab/data/xcom/index.cfm. Gaithersburg, MD: Physics Laboratory, Ionizing Radiation Division; 1998.

National Institute of Standards and Technology. Report of Air-Kerma Calibration. Gaithersburg, MD: Ionizing Radiation Division, Physics Laboratory; 2008.

Olsher R, Eisen Y. A Filter Technique for Optimising the Photons Energy Response of A Silicon PiN Diode Dosimeter. Radiation Protection Dosimetry. 67(4):271-279; 1996.

Storm E, Lier DW, Israel HI. Photon Sources for Instrument Calibration. Health Physics. 26:179-189; 1974.

VITA

Name: David Andrew Wagoner

Address: Department of Nuclear Engineering
Texas A&M University
3133 TAMU
College Station, TX 77843

Email Address: davidwagoner@hotmail.com

Education: B.S., Health Physics, Francis Marion University, 2008
M.S., Health Physics, Texas A&M University, 2010